Cytometry
PART A
Journal of the International Society for Analytical Cytology

Automated Analysis of Neurite Branching in Cultured Cortical Neurons Using HCA-Vision

Pascal Vallotton,[1]* Ryan Lagerstrom,[1] Changming Sun,[1] Michael Buckley,[1] Dadong Wang,[1] Melanie De Silva,[2] Seong-Seng Tan,[2] Jenny M. Gunnersen[2]

[1]CSIRO, Mathematical and Information Sciences, North Ryde, NSW 1670, Australia

[2]Brain Development Laboratory, Howard Florey Institute, University of Melbourne, Parkville, Victoria 3010, Australia

Received 31 May 2007; Revision Received 17 July 2007; Accepted 27 July 2007

This article contains supplementary material available via the Internet at http://www.interscience.wiley.com/jpages/1552-4922/suppmat.

*Correspondence to: Pascal Vallotton, Biotech Imaging, CSIRO Mathematical and Information Sciences, Locked Bag 17, North Ryde, NSW 1670, Australia.

Email: pascal.vallotton@csiro.au

Published online 24 August 2007 in Wiley InterScience (www.interscience.wiley.com)

DOI: 10.1002/cyto.a.20462

Abstract

Manual neuron tracing is a very labor-intensive task. In the drug screening context, the sheer number of images to process means that this approach is unrealistic. Moreover, the lack of reproducibility, objectivity, and auditing capability of manual tracing is limiting even in the context of smaller studies. We have developed fast, sensitive, and reliable algorithms for the purpose of detecting and analyzing neurites in cell cultures, and we have integrated them in software called HCA-Vision, suitable for the research environment. We validate the software on images of cortical neurons by comparing results obtained using HCA-Vision with those obtained using an established semi-automated tracing solution (NeuronJ). The effect of the Sez-6 deletion was characterized in detail. Sez-6 null neurons exhibited a significant increase in neurite branching, although the neurite field area was unchanged due to a reduction in mean branch length. HCA-Vision delivered considerable speed benefits and reliable traces. © 2007 International Society for Analytical Cytology

Key terms

neurite tracing; neurite branching; neurite analysis; neurites; neurite outgrowth; neuron tracing; neuron analysis; cell morphology; neuron image analysis

NEURITE tracing capabilities are invaluable in the drug development arena to identify compounds that display neuroprotective or neuroregenerative effects (1,2). Detailed morphological analyses of neurons are also vital for studying the normal development of dendritic and axonal arbors and for documenting neuropathological changes. Neurite arborization patterns established during development are characteristic for particular neuronal subtypes and relate to function. Neurite arbor size and shape influence the integration of synaptic inputs (3) and these, in turn, are regulated by both intrinsic developmental programs and external signals (4,5). Alterations in neurite arbors have been observed in a number of neuropathological conditions including mental retardation syndromes such as Down, Rett's and Fragile X syndromes (6), schizophrenia (7,8), and Alzheimer's disease (9).

The simplest method for quantifying neurite arbors from digital micrographs involves intensity thresholding. Under controlled imaging conditions, good results can be obtained (10). However, most neurite images display noisy, low contrast areas that affect the ability to detect neurites. A recent implementation of neurite tracing by Xiong et al. used a multi-scale approach, with a Hessian matrix guiding the tracing (11). These authors report measurements of the total length of neurites and of the number of extremities. A system to study neurite dynamics has also been described (12). One of its most interesting features is the ability to correct for relatively frequent tracing mistakes by the use of a probabilistic model, making use of a mask associated with areas where pixel intensities change significantly from image to image.

Here, we present a fully automated image analysis solution for generating neurite traces, for segmenting the cell soma, for associating neurites with their respective

ISAC
International Society for Analytical Cytology

soma, and for producing statistical results on a per-cell basis. We do not attempt to differentiate axons from dendrites. Accordingly, we use the term neurite throughout the manuscript.

Our algorithm is very fast due to its conceptual simplicity (13). Certain elements of our solution are integral to a few commercial platforms in the High Content Analysis industry (14). However, we have found that some applications, such as the analysis of subtle phenotypes, are particularly demanding in terms of tracing quality. Additionally, the variability between images acquired on a research microscope is typically much greater than on a dedicated High Content Analysis instrument. Our solution improves robustness and quality of tracing and still allows on the order of ten images per minute to be processed.

Here, we analyze a representative data set consisting of a total of 101 image fields of embryonic cortical neurons in culture. The comparison was made between seizure-related gene 6 (Sez-6) knockout and wild-type neurons as part of a phenotypic characterization of the Sez-6 knockout mouse line (15). Fifty one wild-type neurons were compared with 50 knockout neurons. Analysis of this data set gives us opportunity to gain a better understanding of the advantages and disadvantages of our fully automated approach and to validate it. These measurements revealed that Sez-6 null neurons display excessive neurite branching.

Our system should allow investigating neurobiological research questions quantitatively at speeds at least one order of magnitude faster than hitherto possible.

Materials and Methods

Cell Culture, Staining, and Imaging

The Sez-6 gene was ablated by homologous recombination in embryonic stem cells followed by transient Cre expression to delete exon I in the process removing transcriptional and translational initiation sites. Embryonic neurons from Sez-6 knockout embryos and wild-type littermate controls were cultured as follows: Embryos (aged 15.5 days) from Sez-6 heterozygous matings were genotyped; cortices from wild-type or Sez-6 knockout embryos were pooled separately and tissue was digested with a Papain Dissociation Kit (Worthington Biochemical Corporation, Lakewood, NJ). For low density cultures, neurons were plated at 1–5 $\times$ 10^4/ml on poly-DL-ornithine/laminin coated coverslips in Neurobasal medium + 2% B27 supplement (Invitrogen, VIC Australia), 0.5 mM glutamine and antibiotics (50 IU/ml penicillin, 50 μg/ml streptomycin). After 5 days in vitro, neurons were fixed (4% paraformaldehyde for 5 min) and immunostained for β-III tubulin (TuJ1; Covance, Richmond, CA; 1/500) using AlexaFluor594–conjugated donkey antimouse IgG (Molecular Probes, Eugene, OR; 1/500) as the secondary antibody to reveal the cell soma and all processes.

Images of neurons were captured using a digital SPOT camera (Diagnostic Instruments, Sterling Heights, MI) mounted on an Olympus inverted microscope model IX 70, with a 40$\times$ objective. An Olympus filter set was used (model U-MWIG). Pixel size in the object space was 0.262 μm and images were 1033 $\times$ 1315 pixels. They were stored and analyzed in uncompressed 8-bit Tiff format.

Image Analysis

In most neuron images, bright and relatively thick primary neurites coexist with dim, thin secondary, and higher order neurites. Additionally, variable labeling efficiency, background fluorescence, and cell debris complicate the task of tracing neurites along their full length using an automated approach. We have developed a robust algorithm based on nonmaximum suppression to delineate neuronal processes (13). The full workflow comprises three stages outlined below and summarized in Table 1. Importantly, only a single set of image analysis parameters was used to analyze the entire image set of 101 image fields. This ensures that the wild type and mutant images are analyzed in exactly the same manner. These parameters are shown in Table 1. They can be set interactively using three software assistants.

Cell Body Detection

In the first assistant, the images of the neurons stained for β-III tubulin are first Gaussian filtered to suppress image noise. They are background corrected using a top hat morpho-

Table 1. Image analysis workflow corresponding to the three assistants described in the text

(A) CELL BODY DETECTION	(B) NEURITE DETECTION	(C) NEURITE ANALYSIS
Smoothing (Gaussian filter: 22 pixels)	Smoothing (Gaussian filter: 15 pixels)	Debarb small branches (13 pixels)
Morphological top hat (background correction: 218 pixels)	Nonmaximum suppression (contrast = 1.5)	Thicken neuron bodies (5 pixels)
Suppression of neurites (morphological opening: 15 pixels)	Removal of small objects (6 pixels)	Remove small trees (4 pixels)
Intensity thresholding (0.62)	Gap closing (9 pixels, quality = 0.75)	Process all tree branches and produce statistics
Object splitting		
Object selection, based on area and border proximity (69, and 65 pixels)		

The values for the single set of image analysis parameters used in this contribution are indicated.

logical filter with a disk structuring element larger than the size of the largest cell body (16). A morphological opening with a structuring element of a diameter smaller than the cell body but larger than all neurites permits suppressing neurite-like structures. Cell bodies are segmented using intensity thresholding with a threshold value selected interactively by the user. The resulting connected regions are then split using a watershed algorithm on the Euclidian distance transform of the images. Smaller objects, for example cell debris, are eliminated based on their smaller sizes.

Neurite Detection Using Nonmaximum Suppression

In the second assistant, the images of the neurons are first Gaussian filtered. We then use nonmaximum suppression to identify linear features. Briefly, the algorithm classifies a pixel as belonging to a linear feature if its intensity is highest among all pixels within a small linear digital neighborhood. This is repeated at a number of orientations (e.g., at 0, 45, 90, and 135°). The operation is repeated for every pixel in the images. The resulting binary mask is then thinned (16). At this stage, connected components smaller than a user defined threshold (typically 4 pixels in diameter) are removed, and gaps in the skeleton are closed using a dynamic programming approach (17). Dynamic programming identifies the shortest path in the image intensity landscape from every extremity of a linear feature to every other linear feature. To limit the extent of connections, a user defined threshold is set on the maximum gap length to bridge. The average intensity value in the original image along the shortest path is computed and a threshold on this parameter is selected to conserve only high quality paths.

Neurite Analysis

In the neurite analysis wizard, the results of the cell body detection and of the neurite detection are combined to produce statistics on a per cell basis. First, very short lateral branches that result from thinning artifacts are removed. Care must be taken to avoid removing genuine, short lateral branches. The appropriate threshold for the length of these branches is set interactively. To that end, the software can toggle between the original image and the segmentation result, while the user is tuning parameters.

Neurite trees are constructed by a process of region growing on a graph. In our representation, the edges of the graph are the branching points of the neurite skeleton, and the nodes are the segments of the skeleton between branch points (See Fig. 2B where each segment is shown in a different color). Region growing begins with segments that touch neuron bodies and continues until all connected segments have been processed. At branch points, the average segment brightness is used to determine priority of the daughter segments, and this in turn produces branch level designations—primary, secondary, tertiary, etc.—for all segments in each neurite tree. This process associates all neurites to their respective parent neurites and cell soma.

Sometimes, a segment close to the cell soma fails to touch it. To avoid losing these segments and the corresponding tree they initiate, cell bodies are thickened using a morphological thickening. Measurements are reported using the nonthickened cell body, both for the cell body and the neurites.

Typical neuron images and the traces produced by the software are shown in Figure 1.

Results

It is important to acquire as many different morphological measures as possible as one does not know in advance the phenotype of a mutation. Over 10 different features are available in HCA-Vision (see Table 2). To validate the quality of traces, we have compared them with results generated semi-manually by a "blind" operator using NeuronJ (18), a popular, semi-automated neurite tracing module of ImageJ (19). NeuronJ finds accurate paths along neurites, with only a few clicks needed to pin the trace to the correct path. Default tracing parameters were used (Version 1.1.0).

The full complement of results for both the automated and the semi-automated traces can be accessed online under the supplementary material. Optimal parameters for the automated analysis were determined using several step by step assistants described in the previous section. In the assistants, sliders trigger image processing almost instantaneously when released. This allowed rapid convergence towards optimal parameter values. A single set of parameters was chosen by experimenting on five images selected at random from images of 101 neurons in total. The actual values used in this contribution are shown in Table 1. The numerical results are shown in Table 2, adjacent to the results from the semi-automated tracing. These results pertain to the full set of 101 fields, including the five images mentioned above.

It took a week to analyze the images semi-automatically compared with only 15 min using HCA-Vision. This represents a gain in time of about two orders of magnitude. Overall, as judged by the results of Table 2, the agreement between the fully automated and the semi automated approaches was excellent.

Discussion

Using HCA-Vision, we obtained results very similar to those obtained by semi-automated tracing. The results support the notion that Sez-6 inhibits neurite branching as the number of branches was significantly higher in neurons lacking Sez-6. On the other hand, the average neurite length was significantly shorter for the Sez-6 knockout neurons, such that the total neurite lengths and neurite fields were not significantly different (see Table 2).

There is considerable biological variability in the results with some neurons displaying total neurite lengths as much as three times those of other neurons within the same class. This stresses the importance of measuring a considerable number of cells in order to reach statistical significance.

There are a number of reasons why slightly different results were obtained using both approaches:

Inaccurate clicking when pinning semi-automated traces to neurites.

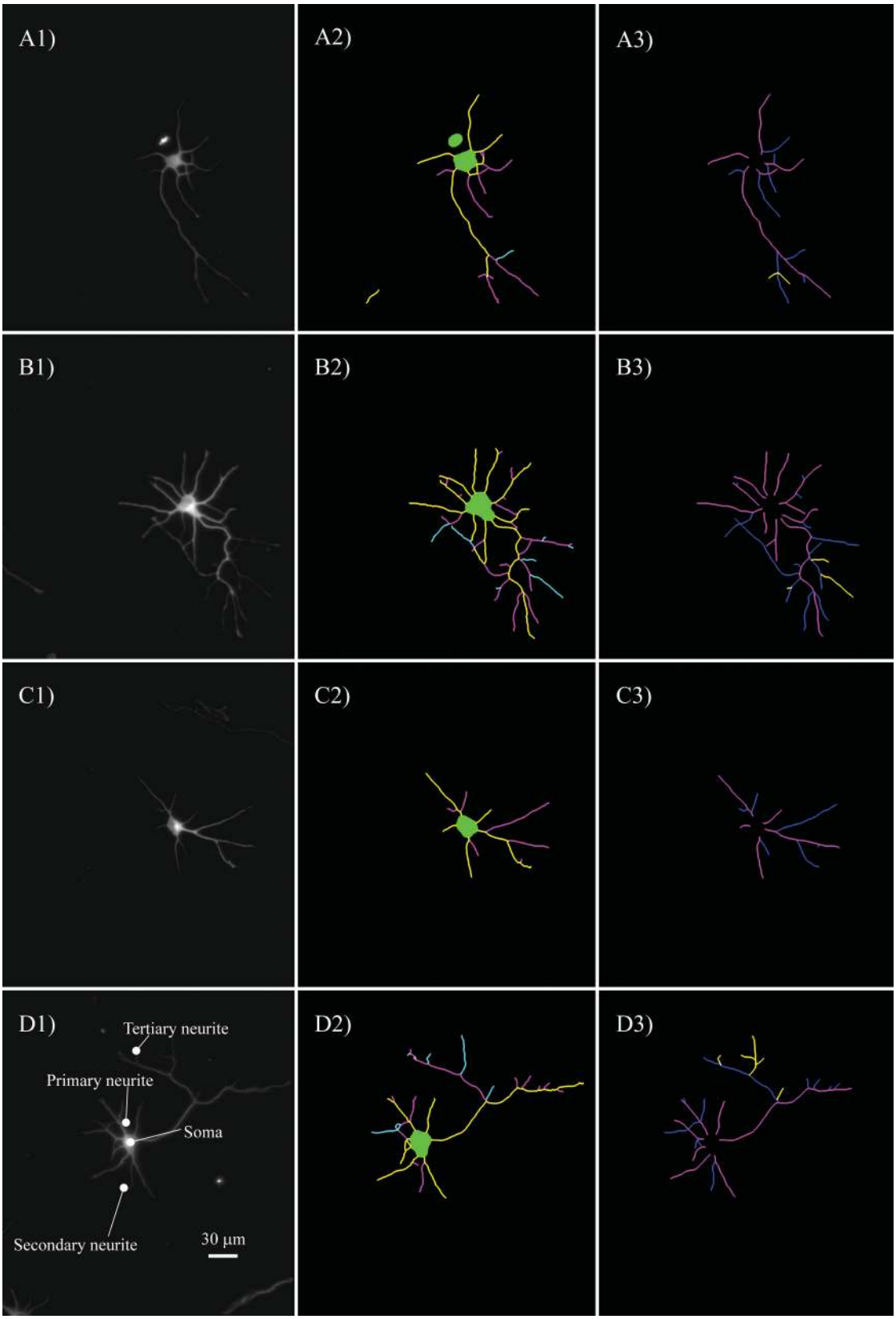

Figure 1. Representative images for Sez-6 knockout (Rows A and B), and wild type neurons (Rows C and D). Column 1: Original images. Column 2: traces obtained using HCA-Vision; primary neurites are yellow, secondary neurites are magenta, and tertiary neurites are cyan. Column 3: results obtained using NeuronJ. Primary neurites are magenta, secondary neurites are blue and tertiary neurites are yellow.

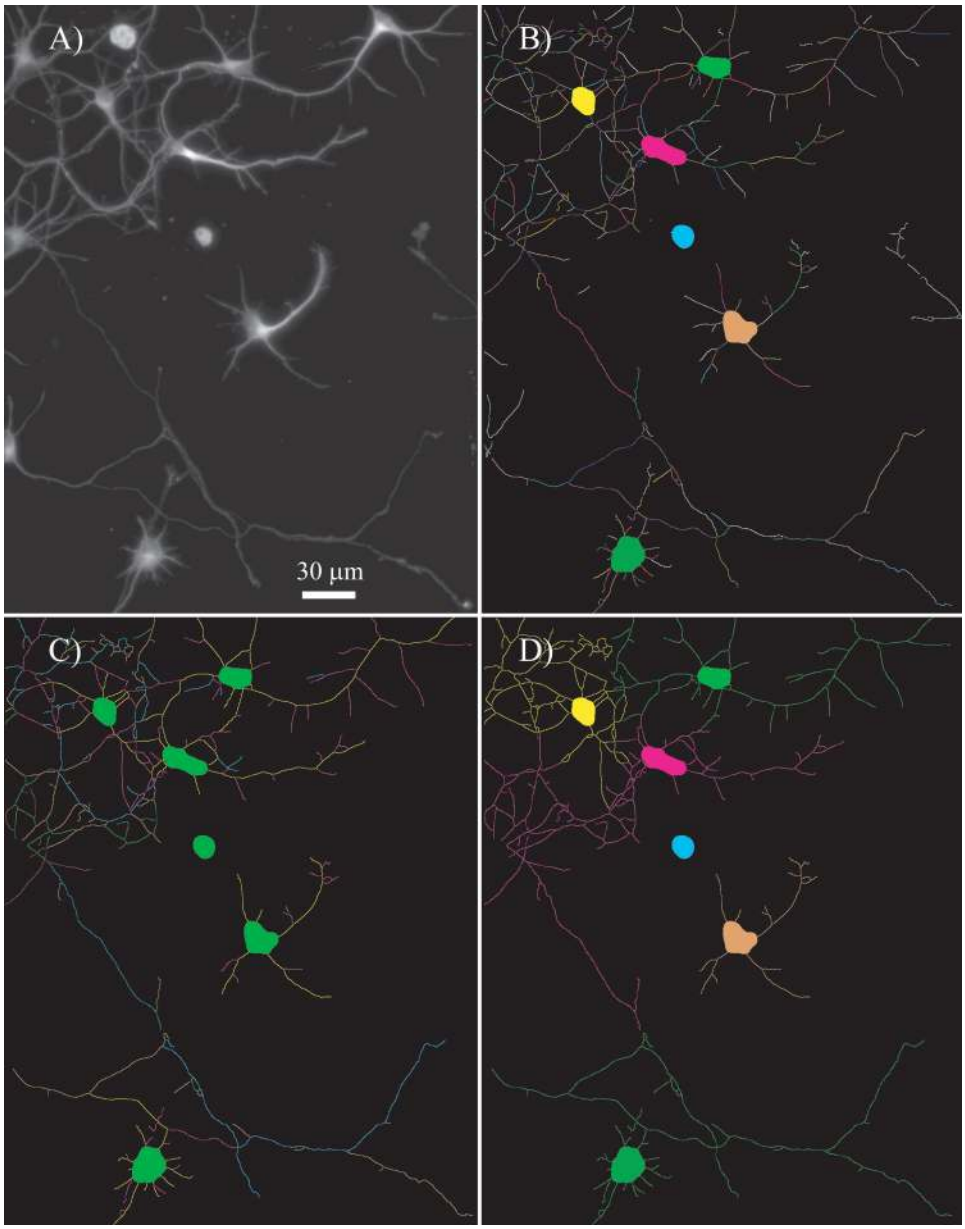

Figure 2. Results produced by HCA-Vision illustrating tracing in high density fields. Only the central cell was used for this manuscript. (**A**) Original image. (**B**) Soma branches image; each segment is in a different color. (**C**) Branch level image; neurites are decomposed among successive branching levels. (**D**) Tree parent image; every cell and all its associated neurites are in a different color. Cell bodies close to the image boundary are automatically removed.

Variable visibility of the neurites on the display. We have found that using alternate software such as IRFANVIEW (20), we could distinguish a few more neurites than in NeuronJ, presumably because of image resampling.

Subjectivity in deciding upon the continuity of neurites at branching points. There is an implicit expectation when tracing neurites semi-manually that tertiary and higher order processes should be short lateral branches. Correspondingly, this suppresses a few very long tertiary processes. In fact, after perusal of the individual images, we could identify outliers that explained the discrepancy (see e.g. frame NeuronJ++54.gif under supplementary material). Using median values instead of averages to report fully automated results decreases the influence of outliers. One obtains 8.43 μm for the wildtype median tertiary length, and 8.22 μm for the knockout median tertiary length. The corresponding measurements for the semi-automated results are 8.34 μm, and 8.75 μm, respectively, in good agreement.

Fully automated tracing occasionally has problems bridging over large fragments of cell debris that lie on a neurite.

Table 2. functionally relevant morphological features for both wild type (++), and sez-6 knockout (−−) embryonic neurons

	FULLY AUTOMATED (HCA-VISION)					SEMI-AUTOMATED (NEURONJ)				
	++		−−			++		−−		
	MEAN	STDM	MEAN	STDM	PVAL	MEAN	STDM	MEAN	STDM	PVAL
Area	206.2	9.2	204.1	9.7	0.88	NA	NA	NA	NA	NA
Perimeter	68.2	2.1	68.8	2.1	0.83	NA	NA	NA	NA	NA
Total neurite length	495.0	28.9	528.3	31.1	0.44	501.9	26.5	536.2	32.5	0.41
Max neurite length	162.3	9.9	126.9	8.5	0.01	152.4	10.6	118.8	7.8	0.01
Max branch layer	2.9	0.1	3.2	0.1	0.07	NA	NA	NA	NA	NA
Mean branch layer	1.5	0.0	1.5	0.0	0.17	NA	NA	NA	NA	NA
Num branch points	10.8	1.1	14.8	1.4	0.03	10.4	0.9	14.7	1.3	0.01
Num of roots	6.3	0.3	8.3	0.3	0.00	6.2	0.3	7.7	0.3	0.00
Num of segments	28.7	2.4	39.0	2.9	0.01	NA	NA	NA	NA	NA
Num of extremities	17.3	1.2	23.4	1.5	0.00	16.6	1.0	22.4	1.4	0.00
Neurite field Area	11324	1049.9	8917.0	712.7	0.06	NA	NA	NA	NA	NA
Max intensity neurite	156.6	7.8	146.2	8.6	0.38	NA	NA	NA	NA	NA
Mean intensity neurite	48.7	1.8	41.6	1.6	0.00	NA	NA	NA	NA	NA
Integrated intensity neurite	113986	8451	105458	8228	0.48	NA	NA	NA	NA	NA
Stdev intensity neurite	26.7	1.2	24.4	1.0	0.15	NA	NA	NA	NA	NA
Lvl1 No branches	6.3	0.3	8.3	0.3	0.00	6.2	0.3	7.7	0.3	0.00
Lvl1 Tot length	274.7	13.4	273.8	14.4	0.97	295.1	14.4	306.9	14.0	0.56
Lvl1 Max length	130.0	9.3	94.3	7.1	0.00	145.7	11.2	116.6	7.8	0.04
Lvl2 No branches	8.3	0.8	11.0	0.8	0.02	8.4	0.7	11.7	0.9	0.01
Lvl2 Tot length	178.7	16.0	198.8	15.0	0.37	180.5	15.9	196.8	17.2	0.49
Lvl2 Max length	73.2	8.6	59.7	7.1	0.23	65.1	7.7	48.3	5.7	0.08
Lvl3 No branches	3.2	0.5	5.0	0.9	0.10	3.1	0.4	3.8	0.5	0.08
Lvl3 Tot length	41.6	10.6	55.6	11.7	0.38	26.2	7.2	32.6	5.8	0.49
Lvl3 Max length	20.8	5.5	18.5	2.5	0.71	13.4	3.4	15.9	2.8	0.58
Max intensity neuron	228.4	5.2	226.9	4.8	0.83	NA	NA	NA	NA	NA
Mean intensity neuron	125.2	3.3	117.8	3.3	0.12	NA	NA	NA	NA	NA
Integrated intensity neuron	385778	22146	358095	21841	0.38	NA	NA	NA	NA	NA
Stdev intensity neuron	46.2	1.3	45.3	1.1	0.59	NA	NA	NA	NA	NA
Mean primary length	45.3	2.3	34.9	2.0	0.00	47.3	2.3	39.9	1.8	0.01
Mean sec length	23.6	2.0	19.2	1.2	0.01	21.4	1.9	16.8	1.5	0.01
Mean tert length	13.6	2.4	9.5	0.8	0.09	8.6	2.4	8.7	1.6	0.63

Stdm, Standard deviation on mean; pval, *p*-value of Student's *t*-test.
Measurements in micrometers pertain to the full set of 101 neuron fields.

Methods for measuring distances on a digital grid may vary from software to software. We used strict Euclidian distances in HCA-Vision.

Occasionally, the software fails to correctly link a tertiary neurite with a secondary neurite for example when the contrast is very low or the branching density high.

The cells for this study were plated at low density to avoid cell–cell contact. Only isolated neurons having no contact with other neurons were analyzed. HCA-Vision also produces results when cells are touching as shown in Figure 2 but these results are more subject to interpretation. In particular, the decision to attribute a neurite touching two cells to either of them is arbitrary. In Figure 2, we also illustrate alternative representations of neurite traces used by the software.

More effort could go into better mimicking the tracing and labeling of neurite branches with reference to an expert user. However, different experts may use slightly different definitions and they may evolve over time. Our fully automated approach, supported by our operational definitions was shown to characterize subtle changes in a consistent and sensitive manner.

In conclusion, HCA-Vision delivered comprehensive structural information very rapidly. The images that were used were representative in their variability of a typical research environment. The tracing capabilities of the software may help uncover subtle phenotypes that had been missed hitherto.

Acknowledgments

We are grateful to Paul Jackway and David Mitchell for helpful comments.

Literature Cited

1. Kim JY, Schafer J, Ming GL. New directions in neuroregeneration. Expert Opin Biol Ther 2006;6:735–738.
2. Kobayashi H, Watanabe E, Murakami F. Growth cones of dorsal-root ganglion but not retina collapse and avoid oligodendrocytes in culture. Dev Biol 1995;168:383–394.
3. Gulledge AT, Kampa BM, Stuart GJ. Synaptic integration in dendritic trees. J Neurobiol 2005;64:75–90.
4. Jan YN, Jan LY. The control of dendrite development. Neuron 2003;40:229–242.
5. Wong RO, Ghosh A. Activity-dependent regulation of dendritic growth and patterning. Nat Rev Neurosci 2002;3:803–812.
6. Kaufmann WE, Moser HW. Dendritic anomalies in disorders associated with mental retardation. Cereb Cortex 2000;10:981–991.
7. Harrison PJ. The neuropathology of schizophrenia. A critical review of the data and their interpretation. Brain 1999;122(Part 4):593–624.
8. Lewis DA, Glantz LA, Pierri JN, Sweet RA. Altered cortical glutamate neurotransmission in schizophrenia: Evidence from morphological studies of pyramidal neurons. Ann NY Acad Sci 2003;1003:102–112.
9. Anderton BH, Callahan L, Coleman P, Davies P, Flood D, Jicha GA, Ohm T, Weaver C. Dendritic changes in Alzheimer's disease and factors that may underlie these changes. Prog Neurobiol 1998;55:595–609.
10. Bilsland J, Rigby M, Young L, Harper S. A rapid method for semi-quantitative analysis of neurite outgrowth from chick DRG explants using image analysis. J Neurosci Methods 1999;92:75–85.
11. Xiong G, Zhou X, Degterev A, Ji L, Wong ST. Automated neurite labeling and analysis in fluorescence microscopy images. Cytometry A 2006;69A:494–505.
12. Al-Kofahi O, Radke RJ, Roysam B, Banker G. Automated semantic analysis of changes in image sequences of neurons in culture. IEEE Trans Biomed Eng 2006;53:1109–1123.
13. Sun C, Vallotton P. Fast linear feature detection using multiple directional nonmaximum suppression. Hong Kong, 20–24 August 2006. Proc Int Conf Pattern Recognit 2006:288–291.
14. Bischof L, Buckley M, Lagerstrom R, Sun C, Talbot H, Wang D, Vallotton P. Image analysis of neurite branching: High-content screening at high speed. Am Biotech Lab 2005;23:22.
15. Gunnersen JM, Kim MH, Fuller SJ, De Silva M, Britto JM, Hammond VE, Louise Faber ES, Sah P, Tan S. Sez-6 proteins affect dendritic arborization patterns and excitability of cortical pyramidal neurons. Neuron (in press).
16. Soille P. Morphological Image Analysis. New York: Springer; 2004.
17. Sun C, Pallottino S. Circular shortest path in images. Pattern Recogn 2003;36:709–719.
18. Meijering E, Jacob M, Sarria JC, Steiner P, Hirling H, Unser M. Design and validation of a tool for neurite tracing and analysis in fluorescence microscopy images. Cytometry A 2004;58A:167–176.
19. Rasband WS. ImageJ, U.S. National Institutes of Health, Available at http://rsb.info.nih.gov/ij/ 1997–2006.
20. Skiljan I. IRFANVIEW, Available at http://www.irfanview.com 2007.